Journal of Power Sources 196 (2011) 2551–2557

Contents lists available at ScienceDirect

Journal of Power Sources

journal homepage: www.elsevier.com/locate/jpowsour

Electrochemical characteristics of samaria-doped ceria infiltrated strontium-doped $LaMnO_3$ cathodes with varied thickness for yttria-stabilized zirconia electrolytes

Dong Ding[a,b], Mingyang Gong[a], Chunchuan Xu[c], Nicholas Baxter[a], Yihong Li[a], John Zondlo[c], Kirk Gerdes[b], Xingbo Liu[a,b,*]

[a] Mechanical and Aerospace Engineering Department, West Virginia University, Morgantown, WV 26506, United States
[b] National Energy Technology Laboratory, Morgantown, WV 26507, United States
[c] Chemical Engineering Department, West Virginia University, Morgantown, WV 26506, United States

ARTICLE INFO

Article history:
Received 14 September 2010
Received in revised form 1 November 2010
Accepted 3 November 2010
Available online 9 November 2010

Keywords:
Doped ceria
Sr-doped $LaMnO_3$ cathode
Infiltration
Yttria-stabilized zirconia
Solid oxide fuel cells

ABSTRACT

Samaria-doped ceria (SDC) infiltrated into strontium-doped $LaMnO_3$ (LSM) cathodes with varied cathode thickness on yttria-stabilized zirconia (YSZ) were investigated via symmetrical cell, half cell, and full cell configurations. The results of the symmetrical cells showed that the interfacial polarization resistance (R_P) decreased with increasing electrode thickness up to ~30 μm, and further increases in the thickness of the cathode did not cause significant variation of electrode performance. At 800 °C, the minimum R_P was around 0.05 Ω cm^2. The impedance spectra indicated that three main electrochemical processes existed, possibly corresponding to the oxygen ion incorporation, surface diffusion of oxygen species and oxygen adsorption and dissociation. The DC polarization on the half cells and characterization of the full cells also demonstrated a similar correlation between the electrode performance and the electrode thickness. The peak power densities of the single cells with the 10, 30, and 50-μm thick electrodes were 0.63, 1.16 and 1.11 W cm^{-2}, respectively. The exchange current densities under moderate polarization are calculated and possible rate-determining steps are discussed.

1. Introduction

Because of its thermal stability and chemical compatibility, Sr-doped $LaMnO_3$ (LSM) is the most commonly used cathode for the yttria-stabilized zirconia (YSZ) electrolyte in solid oxide fuel cells (SOFCs) operating above 800 °C [1,2]. As the performance of the SOFCs is regarded to be primarily restricted by both the ohmic behavior derived from the electrolyte and the interfacial polarization associated mainly with the cathode kinetics [3], extensive research efforts have been devoted to the fabrication of the electrolyte membrane and the development of high-performance cathode materials. Since there have been great advances for YSZ film preparation recently [4–6], it is desirable to develop a high-performance LSM electrode for application as a cathode material in the SOFC.

Construction of a composite cathode is a potentially effective strategy to improve the electrode performance due to the extension of the triple-phase-boundary (TPB) region away from the physical electrolyte/electrode interface [7,8]. Recently, ion-infiltration (or ion-impregnation) methods were widely employed to fabricate composite electrodes, and electrodes so composed were reported to possess high electrocatalytic activity [9–11]. Infiltrated electrodes were also experimentally demonstrated to have larger TPB length compared to conventional composite cathodes due to the introduction of nano-sized oxide particles [12–14].

There are two basic infiltration strategies with respect to the LSM-related cathode [15,16]: one is to infiltrate LSM nano-particles into a single-phase ionic-conducting percolated network [17], while the other is infiltrating ionically conducting species into the LSM backbone [18]. Compared with the former, the infiltrated-LSM cathodes have the advantage of easily forming the desired phase of the infiltration particles [16], and could facilitate fundamental research of the modified LSM cathode. Doped ceria species were usually chosen as an infiltrate due to its high ionic conductivity [19]. Jiang et al. comprehensively studied the Gd-doped ceria (GDC) infiltrated LSM cathodes on YSZ electrolytes in symmetric cell experiments [18,20,21], and they found that a 5.8 mg cm^{-2} GDC infiltrated LSM electrode had a polarization resistance of 0.21 Ω cm^2 at 700 °C, much lower than the baseline LSM electrode having a value of around 12 Ω cm^2. A series of electrochemical char-

* Corresponding author at: Mechanical and Aerospace Engineering Department, West Virginia University, P.O. Box 6106, Morgantown, WV 26506, United States. Tel.: +1 304 293 3111; fax: +1 304 293 6689.
E-mail address: Xingbo.liu@mail.wvu.edu (X. Liu).

0378-7753/$ – see front matter © 2010 Elsevier B.V. All rights reserved.
doi:10.1016/j.jpowsour.2010.11.007

acterizations made by this same group have also demonstrated that GDC infiltration can cause a significant improvement in the electrocatalytic kinetics of the LSM electrode. Unfortunately, there are no reports available associated with doped-ceria infiltrated LSM applied to full cells with YSZ electrolytes. Xia et al. investigated the SDC infiltrated LSM cathode on SDC electrolytes. This work was mainly concerned with the oxygen reduction mechanism [22] and some preparation parameters [23,24]. The peak power density of 0.12 and 0.46 W cm^{-2} was reported at 600 °C when SDC was used as the electrolyte, implying that the infiltrated-LSM electrode is more suitable used at a temperature range of 700 °C and above in which YSZ is more commonly used as the electrolyte.

As mentioned above, the composite electrode may possess a more voluminous electrochemical reaction zone by extending the TPB into the bulk electrode. Increasing the electrode thickness will thus lead to an increase in the TPB length, giving rise to improved electrode performance. However, an increase in the electrode thickness will extend the electronic or ionic conduction path and the gas molecules' diffusion length, resulting in an increase in the electrode ohmic and concentration polarization losses. Most importantly, in the case of the infiltrated cathode, the effect of the infiltrated specie on TPB extension will be predictably limited since the nano-particles are deposited onto the inner surface of pre-formed electrode backbone. Therefore, an optimal thickness corresponding to the minimum electrode polarization resistance will definitely exist. The relationship between the electrode polarization resistance and electrode thickness has been investigated with various models [25–27]. For $Ba_{0.5}Sr_{0.5}Co_{0.8}Fe_{0.2}O_{3-\delta}$ infiltrated GDC cathodes, Nicholas and Barnett [28] used a finite element model to illustrate that the polarization resistance decreases with electrode thickness, and the resistance appears to reach an asymptotic limit at electrode thicknesses greater than ~10 μm for $Ba_{0.5}Sr_{0.5}Co_{0.8}Fe_{0.2}O_{3-\delta}$ infiltrated GDC cathodes. Recently, a particle-layer model proposed by Zhang and Xia [29] predicted that minimum polarization resistances will be achieved for infiltrated cathodes which are thinner than the conventional composite cathode. Experimental studies also described the relationship of electrode performance and thickness. Kenjo et al. [25] found that the electrode polarization resistance decreases with its thickness to a minimum value at the thickness of ~10 μm for LSM–YSZ and 30–40 μm for Pt-$Er_{0.4}Bi_{0.6}O_3$. Juhl et al. [30] reported that the resistance of LSM–YSZ decreases with increasing thickness in the range of 2–12 μm, and the influence of thickness on the electrode resistance is more sensitive at 700 °C and 850 °C compared to 1000 °C. Barbucci et al. [31] performed impedance measurements of the LSM–YSZ composite cathodes possessing different thicknesses. The polarization resistance generally decreases with increasing thickness up to about 40 μm, with a slight increase in polarization for larger thickness. However, no data are reported regarding the infiltrated electrode so far.

In our present work, we investigate the performance of samaria-doped ceria (SDC) infiltrated into strontium-doped $LaMnO_3$ cathodes with various electrode thicknesses on yttria-stabilized zirconia electrolytes. Performance is characterized using symmetrical cell, half cell and full cell test configurations. The electrochemical behaviors of the infiltrated electrodes under open circuit and electrical load were studied, and the cathode reaction kinetics are discussed.

2. Experimental

Symmetrical cells with yttria-stabilized zirconia (YSZ) electrolytes and samaria-doped ceria (SDC) infiltrated into $La_{0.8}Sr_{0.2}MnO_3$ (LSM) cathodes were prepared to determine interfacial polarization resistance (R_P). 8 mol% Y_2O_3 stabilized ZrO_2 powders (8YSZ, Tosoh, SB grade) were uniaxially cold pressed at 400 MPa and sintered at 1450 °C for 5 h to form electrolyte substrate discs approximately 10.5 mm in diameter and 1 mm in thickness. The $La_{0.8}Sr_{0.2}MnO_3$ (LSM) ink was prepared by mixing commercial LSM powder (Nextech, 6.2 m^2 g^{-1}), 10 wt.% graphite as pore former and terpineol in a ceramic 3-roll mill for 30 min. LSM was then screen-printed on both sides of YSZ pellets and sintered at 1100 °C for 2 h to form LSM cathode backbones. The thickness of LSM cathode backbones was increased by sequential screen printing of LSM. The SDC particles were coated onto the inner surface of the porous LSM backbone using an ion-infiltration process. An aqueous-ethanol solution (H_2O:ethanol = 2:3) containing $Ce(NO_3)_3$ and $Sm(NO_3)_3$ (Ce^{3+}:Sm^{3+} = 4:1) was infiltrated into each side of porous LSM electrode, dried at 70 °C, and heated at 800 °C for 2 h to form $Ce_{0.8}Sm_{0.2}O_{1.9}$ particles. All metal nitrates were of analytical grade from the Alfa Aesar chemical reagent company. The SDC loading was determined by weighing the samples before infiltration and after heating, and is defined as the weight percent of SDC in the SDC-infiltrated LSM electrode. Since it is reported that the infiltration loading has a distinct effect on electrode performance, the identical SDC loading weight ratio (50 wt.%) was employed for comparison [14,32]. In our work, a 50 wt.% SDC-infiltrated LSM was found to have a minimum polarization resistance compared with other loadings, which is in agreement with those reported by Jiang et al. [33].

A half cell with a three-electrode configuration was used to measure the overpotential of the SDC-infiltrated LSM electrodes. Here the YSZ electrolyte substrates were about 25 mm in diameter and 1 mm in thickness. A SDC-infiltrated LSM working electrode (WE) was fabricated by the same process as described for the symmetrical cells. The working electrode area was 0.71 cm^2. The counter electrode (CE) was prepared by applying Pt paste (Heraeus Materials Tech. LLC) to the opposite side of the WE on the electrolyte. The Pt reference electrode (RE) was deposited as a ring around WE and the distance between the WE and RE was around 4 mm. After application, both the CE and RE were thermally treated at 800 °C for 30 min.

A full cell consisting of a NiO–YSZ anode substrate, YSZ electrolyte film, and SDC-infiltrated LSM cathode was fabricated for further electrochemical investigation. The bi-layer containing the anode substrate and electrolyte film was fabricated with a spin-coating and co-sintering technique. Anode powders of NiO (NexTech, Standard grade), YSZ (8YSZ, Tosoh, S grade) and the pore former in a weight ratio of 45:45:10 were ball milled for 24 h with ethanol as the medium. The powders were dried at 75 °C overnight, screened with a 120-mesh sieve, and pressed at 140 MPa into green pellets. The pellets were pre-sintered at 1100 °C for 2 h to form the anode substrate. The YSZ-film layer was deposited with a spin coater. The YSZ electrolyte colloidal solution was prepared by ball-milling the YSZ powder in ethanol containing polyvinyl butyral/ethyl cellulose as a binder and polyethyleneimine as a dispersant. After co-sintering of anode/electrolyte at 1450 °C for 5 h, the SDC-infiltrated LSM cathode was prepared using the same process as that described for the half cell. Noted that the thickness of electrolyte is around 10 μm and the area of the cathode is approximately 0.7 cm^2.

Electrochemical impedance spectroscopy (EIS) measurements for symmetrical cells were performed in ambient air under open circuit conditions from 600 to 800 °C, a typical temperature range for intermediate-temperature SOFCs. Impedance spectra were measured in the frequency range of 1 MHz to 0.1 Hz with 20 mV amplitude of the AC signal (SI solatron 1260). The spectra were analyzed using impedance analyzer software (ZsimpWin, PerkinElmer Instruments). The electrode overpotential was measured at 800 °C in conjunction with EIS and DC polarization (SI solatron 1287). The overpotential, η, could be calculated by the following

equation [33]:

$$\eta = U_{WR} - iR_{ohm} \quad (1)$$

where U_{WR} is the stable voltage between WE and RE, obtained when passing a direct current, i, through the half cell for at least 30 min, and R_{ohm} is the ohmic resistance obtained from the high frequency intercept of real axis in the impedance spectrum. The full cells were assembled using the two alumina flanges to mount with compressive mica gasket as seals. Pt meshes were attached to both the anode and the cathode surfaces using nickel and platinum paste, respectively. The detailed test setup was described previously [34,35]. Electrochemical testing was performed at 800 °C with humidified hydrogen (3% H_2O) as the fuel at a flow rate of 200 sccm. The air flow on the cathode side was maintained at 300 sccm. The microstructure and thickness of the cathode was investigated using scanning electron microscopy (SEM, JEOL 7600F).

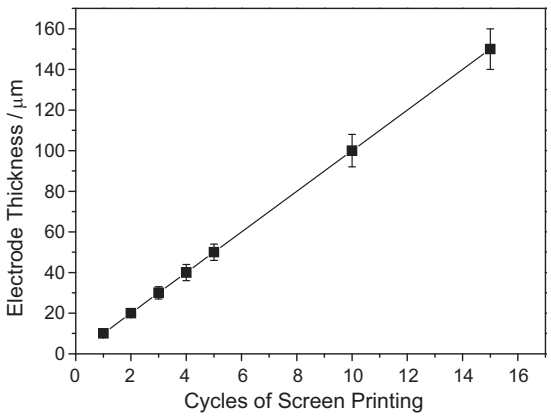

Fig. 1. Dependence of the electrode thickness on cycles of screen printing.

3. Results and discussions

3.1. Cathode thickness determination and microstructure evolution

The correlation between LSM cathode thickness and screen-print cycles is summarized in Fig. 1. One layer of screen print clearly results in a sintered electrode thickness of 10 μm. For sake of establishing linearity, 15 cycles were demonstrated to achieve the 150 μm thick LSM cathode. Fig. 2a and b show the typical SEM images of the LSM baseline cathode and SDC- infiltrated LSM cathode. The pure LSM appears porous and consists of particles with an average particle size of 2 μm. The pore size is about 1–3 μm. After infiltration, LSM particles appear to be covered by film and the interconnection between particles was much closer. Comparative effect of the SDC infiltration is clearly shown in Fig. 2c and d at higher magnification. The deposited particles are nanoscale in size (20–30 nm) and are identified by X-ray diffraction (XRD, Panalytical X'Pert Pro PM-3040) as SDC. Compared with the smooth surface of pure LSM particles, the infiltrated rough surface of LSM particles is coated with mostly spherical SDC particles as a nearly continuous film at 50 wt.% loading.

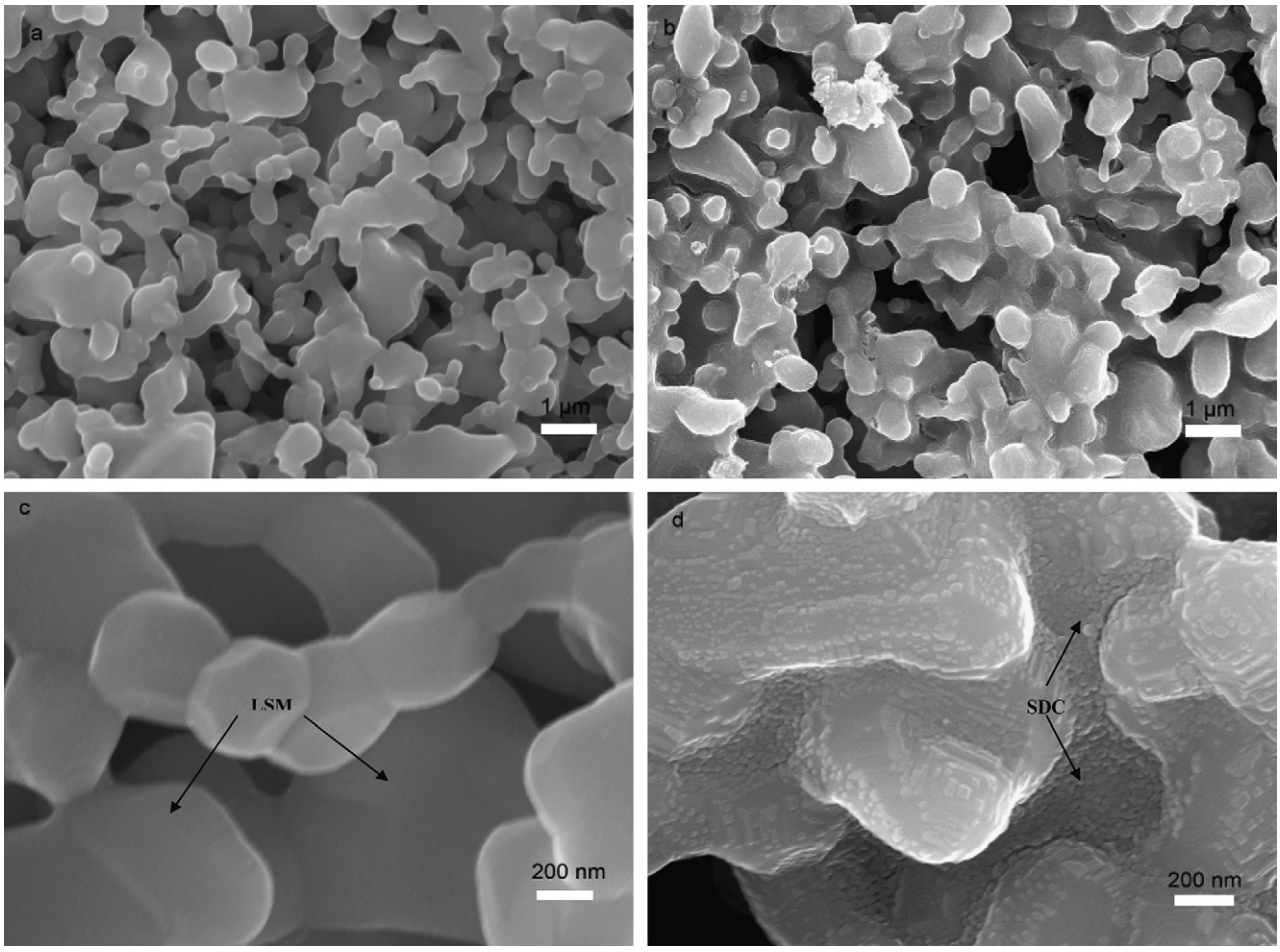

Fig. 2. SEM micrographs of (a) a LSM baseline cathode; (b) a SDC infiltrated LSM cathode; (c) a higher magnification for (a); and (d) a higher magnification for (b).

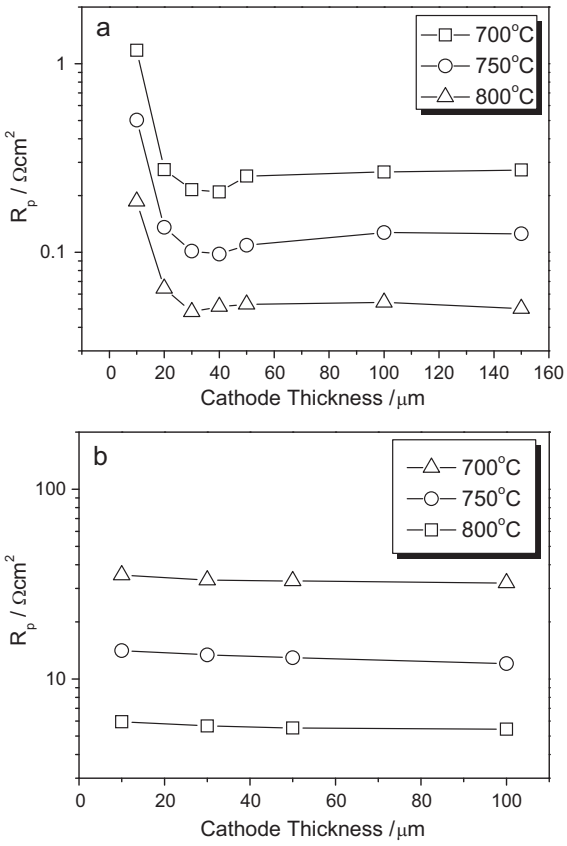

Fig. 3. Correlation between the interfacial polarization resistance and the electrode thickness for: (a) SDC-infiltrated LSM cathodes; and (b) LSM baseline cathodes.

3.2. Electrochemical characterization on symmetrical cells

The relationship between the interfacial polarization resistance and the infiltrated cathode thickness is shown in Fig. 3a. R_P is defined here as half of the difference between the high and low frequency intercept on the real axis of the impedance spectrum. R_P decreases when the electrode thickness increases from 10 to 30 μm, with a slight increase in R_P as thickness further increases up to 50 μm. For example, R_P is 0.186 Ω cm^2 for the electrode with a thickness of 10 μm at 800 °C. It decreases to 0.064 and 0.048 Ω cm^2 as the electrode thickness increases respectively to 20 and 30 μm while the 50 μm thick electrode has a R_P of the 0.053 Ω cm^2. Such variability is very similar to that of conventional LSM–YSZ composite cathodes reported by Barbucci et al. [31]. After the cathode thickness exceeds 50 μm, R_P is nearly constant through tests conducted at increased electrode thickness up to 150 μm, which is 15 times thicker than the thinnest electrode. For sharp contrast to the infiltrated cell behavior, Fig. 3b shows R_P vs. electrode thickness for the pure LSM cathode. The polarization resistance is almost constant at each temperature even as the electrode thickness reaches 100 μm. R_P at 800 °C for the LSM baseline cathode is over 100 times larger than that of the SDC-infiltrated LSM cathode.

Shown in Fig. 4a–g are typical Nyquist plots of the SDC-infiltrated LSM for different cathode thickness measured at 800 °C. It is clear that the infiltrated cathode spectra exhibit invariant frequency distribution as thickness increases, suggesting that the oxygen exchange processes are not sensitive to electrode thickness [33]. The impedance spectra were fitted using an equivalent circuit, as shown in Fig. 4h. Here L is the inductance, R_S is the series resistance assigned to the electrolyte and the lead wires. (RQ) in series represents the arcs appearing at different frequency ranges, in which R is the corresponding resistance and Q the constant phase

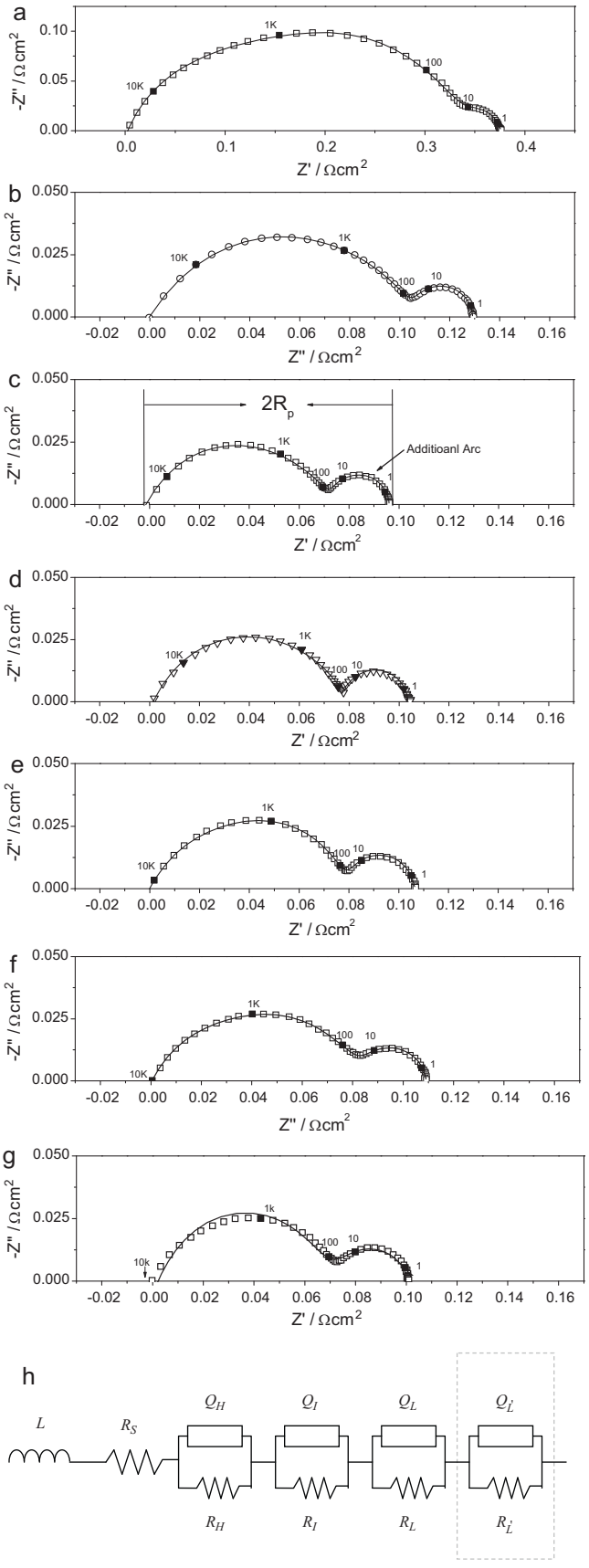

Fig. 4. Typical impedance spectra measured at 800 °C under open circuit for the SDC-infiltrated LSM cathodes with different thickness: (a) 10 μm; (b) 20 μm; (c) 30 μm; (d) 40 μm; (e) 50 μm; (f) 100 μm; and (g) 150 μm; and (h) the equivalent circuit used for fitting these spectra.

element for each arc. Q can be expressed as follows:

$$Q = Y_0(jw)^n \quad (2)$$

where Y_0 is the admittance, w is the angular frequency, and n a frequency exponent. The subscripts H, I, and L refer to the high, intermediate and low frequency arcs. An extra low frequency arc was observed above 700 °C and an additional ($RQ_{L'}$) was thus applied to the circuit. The pseudocapacitance of each (RQ) can be calculated according to the equation:

$$C = Y_0(Y_0R)^{(1-n)/n} \quad (3)$$

Actually, the equivalent circuit shown in Fig. 4h can resolve all impedance spectra over the testing temperature range of 600–800 °C better than using other possible circuits such as two (RQ) in series or a nested or ladder type of two (RQ), also implying the uniformity of electrode process with variation in infiltrated electrode thickness.

Fig. 5a–c shows the temperature dependence of R_H, R_I, and R_L for several electrode thicknesses. The resolved resistances corresponding to high, intermediate and low frequency demonstrated good linear fit when plotted against the reciprocal temperature and also similar activation energy except those derived from 10 μm thick cathode. Noted that at this stage no convincing evidence has been available to be related to this difference in 10 μm thick cathode and those much thicker cathode. R_H decreased with increased electrode thickness. The high frequency arc is possibly derived from the charge transfer processes associated with oxygen ion incorporation from the TPB to the YSZ electrolyte lattice, which is closely related to the TPB length. For the SDC-infiltrated LSM electrodes, additional TPB locations would form and the electrochemically active sites would be extended to the region where LSM, SDC and gas meet. An increase in electrode thickness increases the TPB length (to an optimal limit), establishing more locations for oxygen ion incorporation. This could be further confirmed by the fact that the capacitance increased with electrode thickness. For example, the capacitance measured at 800 °C was 0.15 mF cm^{-2} for the 10 μm thick SDC-infiltrated LSM electrode. It increased to 0.26 mF cm^{-2} for the 30 μm thick electrode and to 0.31 mF cm^{-2} for the 50 μm thick electrode. At the electrode thicknesses of 100 and 150 μm, the capacitances of the high-frequency arcs increased to 0.45 and 0.44 mF cm^{-2}, respectively. It seems that the capacitance is very sensitive to the TPB length since R_P appeared to be constant for thicknesses exceeding 50 μm. In the literatures, there is generally an agreement to attribute the high frequency arc to the O^{2-} incorporation across the electrode/electrolyte interfaces. Kim et al. [36] studied the impedance spectroscopy of an LSM–YSZ composite electrode on YSZ electrolytes, and they found that the capacitance of the high-frequency arc was ~10^{-4} F cm^{-2}, which is similar in value to our results. They attributed such an arc to the O^{2-} incorporation due to a weak P_{O_2} dependence of R_H. Wang et al. [37] also had a similar conclusion. In addition, Wang et al. found that the activation energy of R_H was 1.1 eV as the ionic conducting component in the composite electrodes was relatively high. Their finding is similar to the present results except for the 10 μm thick electrode as shown in Fig. 5a. Furthermore, the high-frequency arc in the present work showed a summit frequency of ~10^4 Hz, which was comparable to a report by Jorgensen and Mogensen [38]. All of these characteristics of the high-frequency arc suggest that our results are in good agreement with those in the literature and it is reasonable to attribute the high-frequency arc to the process of oxygen ion incorporation.

Similar to the high-frequency arc, the intermediate-frequency arc behavior was characterized by a decrease in the resistance (see Fig. 5b) and an increase in the capacitance with coating thickness. The capacitance was 0.84 mF cm^{-2} for the 10 μm thick electrode,

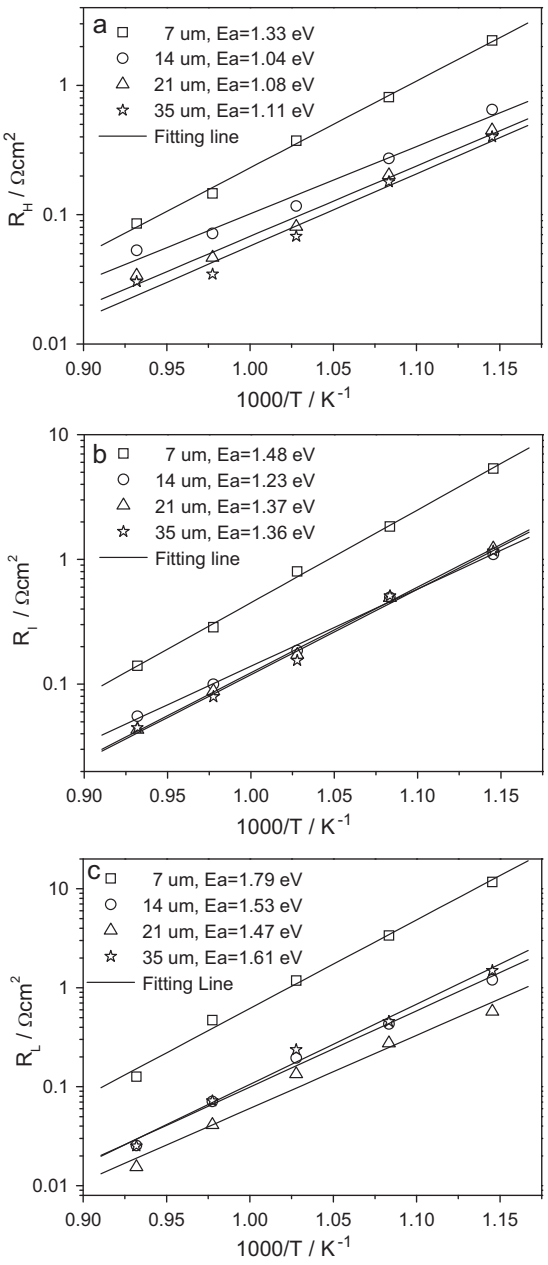

Fig. 5. Dependence of (a) R_H, (b) R_I, and (c) R_L on temperature for the SDC-infiltrated LSM cathodes with varied electrode thickness.

and it was increased to around 1.3 mF cm^{-2} and 1.6 mF cm^{-2} for the 30 μm and 50 μm thick electrodes, respectively. The intermediate-frequency arc showed a summit frequency of 10^2–3×10^3 Hz, in agreement with the results from Jorgensen and Mogensen [38]. In the literatures, dissociative adsorption of oxygen or surface diffusion has been proposed to interpret this kind of arc. In the work of Kim et al. [36], the intermediate-frequency arc was considered to represent O^- surface diffusion due to the experimental evidence of a $P_{O_2}^{1/4}$ dependence. In our following polarization investigation via three-electrode configuration discussed below, the intermediate-frequency arc is confirmed to correspond to surface diffusion of oxygen species along the electrode surface to the TPB area.

The magnitude of the low-frequency arc decreased with increasing electrode thickness as well, and depended strongly on the electrode thickness, which correlates to TPB length. The capacitances of the low-frequency arc increased from 6 mF cm^{-2} to

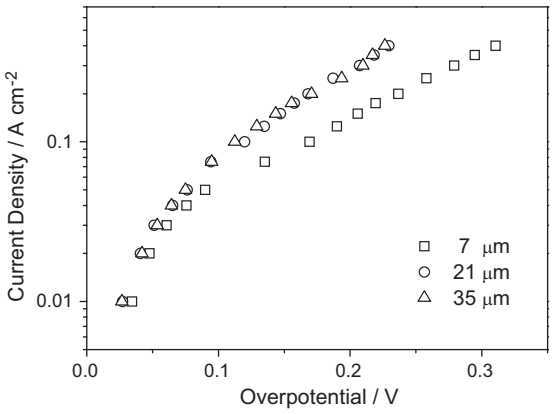

Fig. 6. Cathodic polarization curves of the SDC-infiltrated LSM cathodes with varied electrode thickness.

27 mF cm^{-2} as the electrode thickness increased from 10 μm to 30 μm while the capacitance of the 100 μm thick electrode was as the same as that of the 30 μm thick electrode. The activation energy of R_L was between 1.5 and 1.6 eV, comparable to the values reported by Murray and Barnett [8] who attributed this behavior to the oxygen adsorption and dissociation according to the determination for reaction order of oxygen dependence. The summit frequencies of the low-frequency arc were 10–300 Hz with elevated temperature, suggesting a reasonable agreement with the findings in the literature [39]. Since the arc characteristics in the present work were in accordance with those reported in the literature, this low frequency arc was assumed to be affiliated with dissociative adsorption.

As for the additional low-frequency arc emerging above 700 °C, its magnitude and summit frequency were independent of measurement temperatures. A constant capacitance of 1 F cm^{-2} and a summit frequency of 5 Hz were uniformly observed. Some authors reported the presence of such a low frequency arc with similar characteristics to that seen here and attributed it to gas diffusion [38,40]. Adler et al. also predicted that gas diffusion limitations should be found at lower frequencies than for other processes [41], and some authors demonstrated that gas diffusion played an important role at high temperature just like our case [33].

3.3. Polarization measurement on half cells

Fig. 6 shows the results of DC polarization for the SDC-infiltrated LSM cathode with different electrode thickness measured at 800 °C. The electrode overpotential is usually affected by activation, concentration, and ohmic resistances. The ohmic overpotential is determined by the ohmic resistance, which is the high frequency intercept on the real axis of the impedance spectrum. The overpotential shown in Fig. 6 could be attributed mainly to the activation overpotential since no obvious tendency of limiting current was observed [42]. The polarization performance of the SDC-infiltrated LSM electrodes was enhanced as the electrode thickness increased from 10 μm to 30 μm. Further increase in electrode thickness did not significantly improve the electrode performance. For instance, the overpotential, η, was 169 mV for the 10 μm thick electrode at a cathodic current density of 100 mA cm^{-2}. It decreased to 119 mV and 112 mV for the 30 and 50 μm thick electrode, respectively. This case was in good agreement with the results from the symmetrical cell test.

The exchange current density can be obtained from electrochemical measurements using the AC impedance spectroscopy in conjunction with low-field and high-field approximations to the Butler–Volmer equation as follows [43]:

$$i = i_0 \left[\exp\left(\frac{\alpha_a F\eta}{RT}\right) - \exp\left(\frac{-\alpha_c F\eta}{RT}\right) \right] \quad (4)$$

where i_0 is the exchange current density, F Faraday's constant, R the universal gas constant, T the absolute temperature, and α_a and α_c are the anodic and cathodic charge transfer coefficients, which are related to the number of electrons involved in the overall reaction, n, and the number of times the rate-determining step occurs for one occurrence of the overall reaction, ν, as follows:

$$\alpha_a + \alpha_c = \frac{n}{\nu}$$

When the overpotential is sufficiently low, Eq. (1) reduces to:

$$i = i_0(\alpha_a + \alpha_c)\left(\frac{F\eta}{RT}\right) \quad (5)$$

When the cathodic overpotential is sufficiently high, Eq. (1) is simplified to:

$$i = -i_0 \exp\left(\frac{-\alpha_c F\eta}{RT}\right) \quad (6)$$

and the cathode charge transfer coefficient can be determined from:

$$\alpha_c = \left(\frac{RT}{F}\right)\left(\frac{-1}{\eta}\right) \ln\left|\frac{-i}{i_0}\right| \quad (7)$$

In the low-overpotential region, i_0 could be calculated according to a linear relationship between i and η (assuming $n/\nu = 4/2$). The exchange current density was 33.1, 38.2, and 38.6 mA cm^{-2} for 10, 30, and 50 μm thick electrodes at 800 °C, respectively. The increasing exchange current density versus the electrode thickness demonstrated that increasing the electrode thickness could accelerate the electrode reaction to a certain extent, and an optimal electrode thickness could be achieved around 30 μm for the infiltrated LSM electrodes.

3.4. Typical full cell test

Since the polarization test for the half cells could only be operated at a relatively low overpotential while the electrodes of SOFCs will be normally accompanied with higher current passage in a real condition, it is necessary to investigate the electrochemical performance of the full cell with the SDC-infiltrated LSM cathode at higher current density. Shown in Fig. 7a are the *V–I* and *P–I* curves for the anode-supported full cells with the SDC-infiltrated LSM cathode at various cathode thickness. The peak power densities of the cells with the 10, 30, and 50 μm thick electrode at 800 °C were 0.63, 1.16 and 1.11 W cm^{-2}, respectively. Fig. 7b and c also shows the impedance spectra of the corresponding single cells under open circuit and at a constant potential (vs OCV) of 400 mV, respectively. No matter what conditions the impedance spectra were measured, R_P of the cells significantly decreased as electrode thickness increased from 10 to 30 μm, after which R_p maintained a relatively stable value. This tendency is in good agreement with the results of the symmetrical cell and half cells. McIntosh et al. [44] pointed out that it is difficult to separate the cathodic polarization resistance from anodic one in an anode-supported cell configuration. However, it was reasonable to consider that the variation of R_P originated from that of the cathode since the anodes and electrolytes of all the cells were fabricated similarly. Actually, there is a general agreement that the polarization loss across the interface between electrolyte/cathode dominated the total electrode reaction for anode-supported or electrolyte-supported cells especially at 700 °C and above [4,45,46]. The present work further confirmed this finding. Note that although there is a slight difference of high-frequency intercept in impedance spectra between the cell with

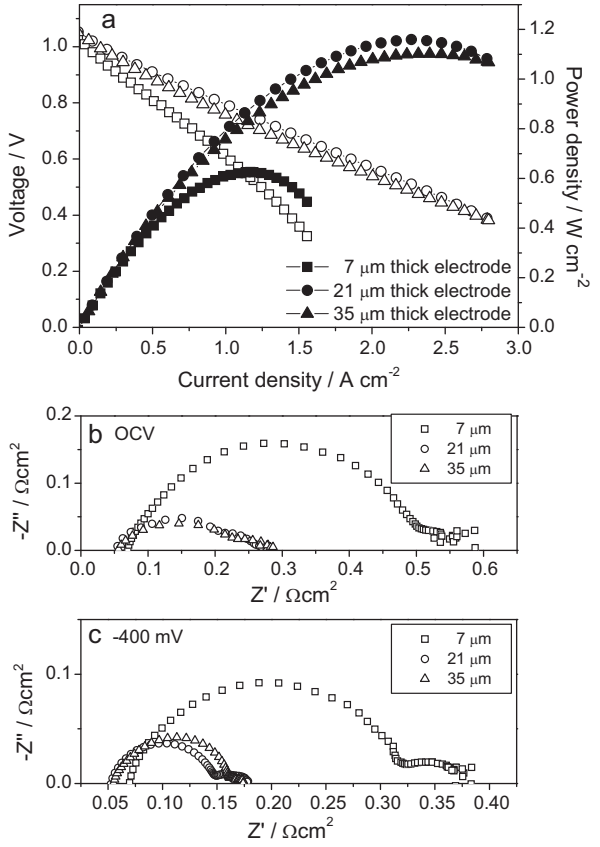

Fig. 7. (a) Performance of the full cells with the SDC-infiltrated LSM cathodes at different electrode thickness; and the corresponding electrochemical impedance spectra measured under (b) open circuit; and (c) at 400 mV vs OCV at 800 °C.

10 μm thick electrode and the cells with thicker electrodes, it is not the main source of the variation in the cell performance when compared with that of R_P.

4. Concluding remarks

In the present work, electrochemical characteristics of samaria-doped ceria (SDC)-infiltrated strontium-doped $LaMnO_3$ (LSM) cathodes with varied thickness on yttria-stabilized zirconia (YSZ) were studied. The results showed that the electrode performance was enhanced with increasing electrode thickness up to ~30 μm, and further increases in the thickness did not cause significant variation of electrode performance in the symmetrical cell, the half cell, or the full cell configuration. Three main electrochemical processes were found in the electrochemical spectra, possibly corresponding to the oxygen ion incorporation, surface diffusion of oxygen species and oxygen adsorption and dissociation. The electrochemical performance of the full cell showed significant improvement as the cathode thickness increased from 10 to 30 μm and a maximum power density of over 1.1 W cm^{-2} was measured at 800 °C.

Acknowledgement

This technical effort was performed in support of the National Energy Technology Laboratory's on-going research on solid oxide fuel cell in West Virginia University.

References

[1] N.Q. Minh, J. Am. Ceram. Soc. 76 (1993) 563–588.
[2] J. Fleig, Annu. Rev. Mater. Res. 33 (2003) 361–382.
[3] S.B. Adler, Chem. Rev. 104 (2004) 4791–4843.
[4] S. De Souza, S.J. Visco, L.C. De Jonghe, J. Electrochem. Soc. 144 (1997).
[5] J.W. Kim, A.V. Virkar, K.Z. Fung, K. Mehta, S.C. Singhal, J. Electrochem. Soc. 146 (1999) 69–78.
[6] R.Q. Yan, D. Ding, B. Lin, M.F. Liu, G.Y. Meng, X.Q. Liu, J. Power Sources 164 (2007) 567–571.
[7] C.W. Tanner, K.Z. Fung, A.V. Virkar, J. Electrochem. Soc. 144 (1997) 21–30.
[8] E.P. Murray, S.A. Barnett, Solid State Ionics 143 (2001) 265–273.
[9] R.J. Gorte, S. Park, J.M. Vohs, C.H. Wang, Adv. Mater. 12 (2000) 1465–1469.
[10] S.P. Jiang, Mater. Sci. Eng. A-Struct. Mater. Properties Microstruct. Process. 418 (2006) 199–210.
[11] D. Ding, Z.B. Liu, L. Li, C.R. Xia, Electrochem. Commun. 10 (2008) 1295–1298.
[12] D. Ding, W. Zhu, J.F. Gao, C.R. Xia, J. Power Sources 179 (2008) 177–185.
[13] W. Zhu, D. Ding, C. Xia, Electrochem. Solid State Lett. 11 (2008) B83–B86.
[14] Z.Y. Jiang, L. Zhang, K. Feng, C.R. Xia, J. Power Sources 185 (2008) 40–48.
[15] T.Z. Sholklapper, H. Kurokawa, C.P. Jacobson, S.J. Visco, L.C. De Jonghe, Nano Lett. 7 (2007) 2136–2141.
[16] Z. Jiang, C. Xia, F. Chen, Electrochim. Acta 55 (2010) 3595–3605.
[17] C. Lu, T.Z. Sholklapper, C.P. Jacobson, S.J. Visco, L.C. De Jonghe, J. Electrochem. Soc. 153 (2006) A1115–A1119.
[18] S.P. Jiang, Y.J. Leng, S.H. Chan, K.A. Khor, Electrochem. Solid State Lett. 6 (2003) A67–A70.
[19] B.C.H. Steele, P.H. Middleton, R.A. Rudkin, Solid State Ionics 40-1 (1990) 388–393.
[20] S.P. Jiang, W. Wang, J. Electrochem. Soc. 152 (2005) A1398–A1408.
[21] S.P. Jiang, W. Wang, Solid State Ionics 176 (2005) 1351–1357.
[22] X.Y. Xu, Z.Y. Jiang, X. Fan, C.R. Xia, Solid State Ionics 177 (2006) 2113–2117.
[23] L. Zhang, F. Zhao, R.R. Peng, C.R. Xia, Solid State Ionics 179 (2008) 1553–1556.
[24] R.F. Tian, J. Fan, Y. Liu, C.R. Xia, J. Power Sources 185 (2008) 1247–1251.
[25] T. Kenjo, S. Osawa, K. Fujikawa, J. Electrochem. Soc. 138 (1991) 349–355.
[26] S. Sunde, J. Electrochem. Soc. 143 (1996) 1930–1939.
[27] S.H. Chan, K.A. Khor, Z.T. Xia, J. Power Sources 93 (2001) 130–140.
[28] J.D. Nicholas, S.A. Barnett, J. Electrochem. Soc. 156 (2009) B458–B464.
[29] Y. Zhang, C. Xia, J. Power Sources 195 (2010) 4206–4212.
[30] M. Juhl, S. Primdahl, C. Manon, M. Mogensen, J. Power Sources 61 (1996) 173–181.
[31] A. Barbucci, M. Carpanese, A.P. Reverberi, G. Cerisola, M. Blanes, P.L. Cabot, M. Viviani, A. Bertei, C. Nicolella, J. Appl. Electrochem. 38 (2008) 939–945.
[32] X.Y. Lou, S.Z. Wang, Z. Liu, L. Yang, M.L. Liu, Solid State Ionics 180 (2009) 1285–1289.
[33] Z.Y. Jiang, L. Zhang, L.L. Cai, C.R. Xia, Electrochim. Acta 54 (2009) 3059–3065.
[34] C.C. Xu, J.W. Zondlo, H.O. Finklea, O. Demircan, M.Y. Gong, X.B. Liu, J. Power Sources 193 (2009) 739–746.
[35] M.Y. Gong, D. Bierschenk, J. Haag, K.R. Poeppelmeier, S.A. Barnett, C.C. Xu, J.W. Zondlo, X.B. Liu, J. Power Sources 195 (2010) 4013–4021.
[36] J.D. Kim, G.D. Kim, J.W. Moon, Y.I. Park, W.H. Lee, K. Kobayashi, M. Nagai, C.E. Kim, Solid State Ionics 143 (2001) 379–389.
[37] S.Z. Wang, Y. Jiang, Y.H. Zhang, J.W. Yan, W.Z. Li, Solid State Ionics 113 (1998) 291–303.
[38] M.J. Jorgensen, M. Mogensen, J. Electrochem. Soc. 148 (2001) A433–A442.
[39] E.P. Murray, T. Tsai, S.A. Barnett, Solid State Ionics 110 (1998) 235–243.
[40] H. Yokokawa, T. Horita, N. Sakai, T. Kawada, M. Dokiya, in: U. Bossel (Ed.), Proceedings of the 1st European SOFC forum, Lucerne, Switzerland, 1994, p. 425.
[41] S.B. Adler, J.A. Lane, B.C.H. Steele, J. Electrochem. Soc. 143 (1996) 3554–3564.
[42] A.C. Co, S.J. Xia, V.I. Birss, J. Electrochem. Soc. 152 (2005) A570–A576.
[43] S.H. Wang, X.Y. Lu, M.L. Liu, J. Solid State Electrochem. 6 (2002) 384–390.
[44] S. McIntosh, J.M. Vohs, R.J. Gorte, J. Electrochem. Soc. 150 (2003) A1305–A1312.
[45] Y. Jiang, A.V. Virkar, F. Zhao, J. Electrochem. Soc. 148 (2001) A1091–A1099.
[46] E. Ivers-Tiffee, A. Weber, D. Herbstritt, J. Eur. Ceram. Soc. 21 (2001) 1805–1811.